Sensitivity of the Latitude of the Surface Westerlies to Surface Friction

Gang Chen *

Program in Atmospheric and Oceanic Sciences, Princeton University,

Princeton, New Jersey

Isaac M. Held

NOAA/Geophysical Fluid Dynamics Laboratory,

Princeton, New Jersey

Walter A. Robinson

Department of Atmospheric Sciences, University of Illinois at Urbana-Champaign,

Urbana, Illinois

September 9, 2006

*Corresponding author address: Gang Chen, Program in Atmospheric and Oceanic Sciences, Princeton University, Princeton, NJ, 08544. E-mail: gchen@princeton.edu

Abstract

The sensitivity to surface friction of the latitude of the surface westerlies and the associated eddy-driven mid-latitude jet is studied in an idealized dry GCM. The westerlies move polewards as the friction is reduced in strength. An increase in the eastward phase speed of midlatitude eddies is implicated as playing a central role in this shift.

This shift in latitude is mainly determined by changes in the friction on the zonal mean flow rather than the friction on the eddies. If the friction on the zonal mean is reduced instantaneously, the response reveals two distinctive adjustment time scales. In the fast adjustment over the first 10-20 days, there is an increase in the barotropic component of zonal winds and a substantial decrease in the eddy kinetic energy; the shift in the surface westerlies and jet latitude occurs in a slower adjustment. The space-time eddy momentum flux spectra suggest that the key to the shift is a poleward movement in the subtropical critical latitude associated the faster eastward phase speeds in the dominant midlatitude eddies. The view is supported by simulating the upper tropospheric dynamics in a stochastically stirred nonlinear shallow water model.

1. Introduction

An understanding of the factors that control the latitude of the surface westerlies has risen to central importance in climate theory, due to observations of a poleward shift in recent years in the Southern Hemisphere (Thompson and Solomon 2002) and the prediction of poleward movement in both hemispheres in response to global warming in the future (Fyfe et al. 1999; Kushner et al. 2001; Miller et al. 2006). This poleward shift, accompanied by zonal wind changes of an equivalent barotropic structure in the troposphere, is often referred to as a shift towards a more positive phase of an annular mode. Idealized models generate poleward shifts in the westerlies in response to increases in stratospheric temperature gradients (Polvani and Kushner 2002; Kushner and Polvani 2004; Haigh et al. 2005), increases in surface temperature gradients (Son and Lee 2005), increases in water vapor and the associated latent heating (Frierson et al. 2006), and increases in the height of the tropopause (Williams 2006). Comprehensive GCM experiments also generate poleward shifts in response to the development of the ozone hole in the Southern hemisphere (Gillett and Thompson 2003), and in response to stratospheric cooling/tropospheric heating (Rind et al. 2005). An understanding of the observed and projected shifts in the westerlies will require critical evaluation of models of all these effects.

We focus here on a particularly simple way of shifting the westerlies in an atmospheric model: changing the strength of surface friction. As the strength of surface drag is reduced, the surface westerlies and the midlatitude jet move polewards (Robinson (1997), hereafter R97). We use this problem as a test case for our understanding of the controls on the midlatitude eddies and the associated mean flows, as it remains

a challenge to identify and isolate cleanly the dynamical mechanisms underlying this shift. Our hope is that the understanding gained will help in the analysis of some of the factors of more direct relevance for climate sensitivity mentioned above.

The sensitivity to surface friction is itself potentially relevant to an understanding of model biases. There is considerable dynamical similarity between the response to changes in surface friction and the response to changes in orographic gravity wave drag (Robinson 1997). As orographic gravity wave drag is introduced to prevent excessive strength of the low level westerlies, these westerlies are simultaneously displaced equatorward (Stephenson 1994). The westerlies are often biased equatorward in comprehensive GCMs (Russell et al. 2006), so this added displacement is generally undesirable. A better understanding of the effects of various types of momentum exchange with the surface on the latitude of the westerlies should be of value for model development.

The surface westerlies can be thought of as marking the location of the dominant region of baroclinic eddy generation: to the extent that wave activity radiates away from this source, eddy momentum fluxes converge into this region, and this momentum is removed from the atmosphere by surface friction through the generation of surface westerlies. Using a global two level primitive equation model, R97 argues that a reduction in surface drag results, first of all, in an enhancement of the barotropic component of the flow, with relatively modest changes in the baroclinic component. But these changes in barotropic meridional shears then modify the eddy heat and momentum fluxes in such a way as to move them polewards, along with the surface westerlies balanced by the momentum flux convergence.

One starting point for thinking about this issue is the analysis of linear baroclinic normal modes and nonlinear baroclinic eddy life cycles. As the barotropic shear increases, linear baroclinic instability is suppressed and eddy fluxes tend to be more confined meridionally, effects referred to as the "barotropic governor" (James 1987). R97 suggests that this mechanism is more active on the equatorward side of the mid-latitude storm track, resulting in stronger suppression on the equatorward side and poleward displacement of the eddies.

Barotropic meridional shear can have a strong effect on baroclinic eddy life cycles and the resulting mean flow modification. Simmons and Hoskins (1980) and Thorncroft et al. (1993) vary the barotropic shear on the equatorward flank of the jet in the initial condition, and obtain two distinct types of life cycle (LC). In LC1, the wave breaking is primarily on the anticyclonic side of the jet, and the final jet position moves to the poleward flank of the initial jet. In LC2, with enhanced cyclonic shear in the initial condition, waves break on the cyclonic side of the jet, and the jet is displaced slightly equatorward. Therefore, changes in the factors that control eddy life cycles which favor LC1 over LC2, such as the increased anticyclonic shear equatorward of the jet, should shift the jet polewards. Hartmann and Zuercher (1998) gradually increase the barotropic shear and find that the transition from LC1 to LC2 is abrupt at a critical value of the strength of the added shear. Thorncroft et al. (1993) and Hartmann and Zuercher (1998) suggest that the type of the wave breaking and the direction of the jet shift can be understood in terms of Rossby wave refraction and reflection. Orlanski (2003), in contrast, finds that a transition from LC1 to LC2 can be obtained in a shallow water model by increasing the amplitude of the forcing, and shows high

resolution life cycles in dry and moist 3D atmospheres that highlight this amplitude effect.

The mid-latitude storm tracks are composed of many growing and decaying waves, often having a non-modal character. Rather than thinking in term of linear modes or nonlinear life cycles initialized with normal modes, one can try to think in terms of stochastically generated variability (see the review by Delsole (2004)). As shown by Delsole (2001), the climatological eddy momentum fluxes can be rather well simulated in the simplest linear stochastically driven barotropic model. It is natural to ask if a model of this type can be constructed to help explain the sensitivity of the westerlies to surface friction.

We have examined the sensitivity of the circulation to surface friction in the idealized dry GCM presented in Held and Suarez (1994), hereafter HS, confirming the robustness of the conclusions in R97. We then attempt to capture the essence of this shift in a stochastically stirred nonlinear shallow water model. The changes in the space-time spectra in the idealized GCM suggest to us that an increase in the characteristic eastward phase speed of the eddies is a key component of the response. This increase in phase speed can be attributed to the increase in the barotropic component of the flow following the decrease in surface drag. We examine the consequence of this increase in phase speed by manipulating the stirring in the shallow water model. The result is indeed a poleward shift in the convergence of the eddy momentum flux that we can think of, at least qualitatively, as due to a shift in the subtropical critical latitude.

The paper is organized as follows. In section 2, we describe the climatological

jet shift as a function of surface friction in the HS model, particularly comparing the relative importance of the drag on zonal mean winds and the drag on the eddies. In section 3, we examine the transient response to an instantaneous change in the surface drag and the resulting changes in eddy-mean flow interaction, distinguishing between relatively fast and slow components of the response. In section 4, we examine the eddy flux spectra as a function of latitude and angular phase speed, and speculate on the importance of the shift in the subtropical critical latitude. In section 5, we describe the shallow water model of the upper troposphere. The details of the shallow water model configuration are included in the appendix. We offer brief discussions and conclusions in section 6.

2. Mean drag versus eddy drag

We use a spectral dry dynamical core, forced by zonally symmetric Newtonian relaxation to the prescribed equilibrium temperature field and damped by Rayleigh friction near the surface, as in HS. The model is run at T42 and T85 horizontal resolutions with 20 equally spaced sigma levels in the vertical. The model output is sampled daily, and the time averaged results are averaged over the last 1600 days of 2000 day integrations.

In the HS formulation, the boundary layer in the momentum equation is simply represented by linear Rayleigh damping in the lower troposphere. The vertical structure of the damping rate is prescribed, decreasing linearly from its value at the surface to zero at $\sigma = 0.7$. This vertical structure is unchanged in all of our simulations. References in the following to the damping time scale refer to the value at the surface. The hyperdiffusion (∇^8) is set so that the diffusive damping time of the smallest retained

spherical harmonic is 0.1 days.

Whereas linear friction damps the zonal mean flow and the zonally asymmetric eddies equally in HS, R97 shows that the jet shift is mainly controlled by the friction on the zonal mean in the two-layer model examined. Hence, we separate the boundary layer drag into the drag on the zonal mean flow (mean drag) and the drag on the eddies (eddy drag).

$$D = -\frac{\bar{u}}{\tau_{fz}} - \frac{u'}{\tau_{fe}} \quad (1)$$

$$= -\frac{u}{\tau_f}, \quad (\text{ only if } \tau_{fe} = \tau_{fz}) \quad (2)$$

Overbars and primes denote the zonal means and the deviations from zonal means; τ_{fz} is the mean damping time and τ_{fe} is the eddy damping time. We use the symbol τ_f when the damping times τ_{fz} and τ_{fe} are equal. As in HS, the control value for the frictional damping time at the surface is 1.0 day.

We first examine the resolution dependence of the model sensitivity to the surface drag. Figure 1 shows the surface (lowest model level) winds at T42 and T85 resolutions for experiments in which τ_f is increased to 1.5 and decreased to 0.5. We also show simulations in which τ_{fe} is varied over this same range, holding τ_{fz} fixed at the control value, and in which τ_{fz} is varied holding τ_{fe} fixed. The strength of the subgrid scale diffusion is modified when the resolution is changed so as to maintain the same diffusive damping time for the smallest resolved spherical harmonic.

We conclude that T42 is sufficient for our study. In both T42 and T85, as the eddy/mean/total damping time increases (surface friction decreases), the extratropical

westerlies and tropical easterlies are intensified, and the extratropical westerlies are displaced poleward. The only significant departure is for the case of increased eddy damping, where there is a larger equatorward shift in the higher resolution model. Also evident from this figure is that the effects of the change in drag are captured relatively well by changing the mean drag only, as in R97.

[Figure 1 about here.]

Using the T42 model, the changes of the atmospheric circulation are displayed in Figs 2 and 3 as a function of mean drag, eddy drag and total drag, varying the damping time over the range 0.25 to 1.75 in increments of 0.25. We show the upper tropospheric zonal mean winds (σ=0.275) and the lower tropospheric zonal mean winds ($\sigma = 0.875$) in Fig. 2, and the globally averaged eddy and zonal mean kinetic energies in Fig. 3. As the mean drag is reduced, the poleward movement of the surface westerlies is continuous over the entire range of damping rates displayed. The upper level eddy driven jet moves polewards continuously as well. For small mean drag, the eddy driven jet in the upper troposphere separates distinctly from the subtropical jet, which is weak in this model due, in part, to the weakness of the tropical heating. Zonal mean kinetic energy K_M is naturally strengthened as the mean drag is reduced, but the eddy kinetic energy K_E is weakened, as expected from the barotropic governor mechanism. Inspection of the model energy cycle (not shown) indicates that the conversion of potential to kinetic energy changes only slightly, while the barotropic conversion increases, despite the reduction in eddy kinetic energy, due to the increased meridional shears.

The dependence on eddy damping is more complex. There is an equatorward

movement as the drag is increased from its control value, but this movement is fairly abrupt as a function of the damping rate; as the drag is decreased from the control value, there is relatively little movement. The abruptness is related to the separation of the storm track from the subtropical jet as the damping is reduced. Before this separation, the flow attempts to squeeze an eddy source and the associated surface westerlies into high latitudes, but this is ill-defined. This abrupt character here might be responsible for the difference in the T42 and T85 resolutions as the eddy damping is increased in Fig 1b. Also it may be related to that found in the jet mergers discussed in the QG context (Panetta 1993; Lee 1997), and by Lee (2005) for a spherical primitive equation model.

[Figure 2 about here.]

If the changes in damping parameters are small, we should be able to predict the changes in climate as the total drag is modified from the corresponding runs in which the mean drag and eddy drag are modified separately. For example, for the globally averaged eddy or zonal mean kinetic energy,

$$\frac{\partial E(\tau_f)}{\partial \tau_f}\delta\tau_f \approx \frac{\partial E(\tau_{fz}, \tau_{fe}=\tau_0)}{\partial \tau_{fz}}\delta\tau_{fz} + \frac{\partial E(\tau_{fz}=\tau_0, \tau_{fe})}{\partial \tau_{fe}}\delta\tau_{fe} \qquad (3)$$

where τ_0 is the control value of surface drag, and the higher order terms are neglected. As seen in Fig. 3, this linear decomposition matches the total drag runs rather well. A key observation is that the effects of the mean drag and eddy drag on K_E are opposite and largely cancel when the two parameters are varied simultaneously. Therefore, when one varies the total drag, one is seeing the combined effects of two rather differ-

ent dynamical mechanisms. Despite its seeming artificiality, we follow R97 in finding it important to separate these two mechanisms. The effects of varying mean damping are responsible for a large fraction of the total response, and do not involve the rather abrupt behavior of the model when eddy damping is increased. Therefore, we choose to focus on the effects of mean damping.

[Figure 3 about here.]

If one linearizes Eq. (1) about the control values of the time and zonally averaged zonal winds $< \bar{u}_0 >$ and surface drag τ_0, and assumes that the deviations are small, one obtains.

$$-\delta(\frac{\bar{u}}{\tau_{fz}}) \approx - < \bar{u}_0 > \delta(\frac{1}{\tau_{fz}}) - \frac{\delta\bar{u}}{\tau_0} \tag{4}$$

The first term is equivalent to the addition of a constant zonal mean torque proportional to the control surface winds and applied within the boundary layer. To test whether this term dominates the results, rather than changing the surface friction, we add a torque to the model of the strength and structure corresponding to this first term, using the frictional damping difference between the 1.0 and 1.5 day. The surface wind response to this torque is compared in Fig. 4 with the surface wind change as the mean drag is reduced from 1.0 to 1.5 day. While the response of surface winds is slightly less poleward and weaker in the case of the imposed torque, the two cases agree rather well. This result implies that the surface wind displacement can be thought of, qualitatively at least, as a response to an imposed zonal mean torque.

[Figure 4 about here.]

3. The transient response to a change in the mean drag

Although we perturb the surface friction on the eddies and zonal mean flow separately, the equilibrated response does not answer the question of cause and effect in the eddy-mean flow interaction. As a start in addressing causality, it is useful to examine the adjustment of the eddies and zonal means in the time-dependent response to a sudden reduction in the mean drag. Starting from the equilibrated state with the 0.5 day mean drag, we increase the mean damping time to 1.5 day and run the model until it equilibrates. The same experiment is repeated with 30 different initial conditions selected from the run with 0.5 day damping. The evolution of the ensemble mean is displayed in Fig. 5.

[Figure 5 about here.]

The figure illustrates vividly two distinctive adjustment time scales. In days 0-15, the fast adjustment, the mean kinetic energy, K_M, increases in response to the weaker mean drag while the eddy kinetic energy, K_E, decreases. Thus, the barotropic governor effects act quickly, but with little effect on the jet position. The poleward jet shift occurs mostly in the slow adjustment, days 15-300, accompanied by further increase in the zonal mean kinetic energy with an e-folding time of roughly 50 days.

Figure 6 shows the vertical structure of zonal wind changes during the fast and slow adjustments. In days 0-15, the extratropical winds at all levels in the troposphere follow the increase of the surface westerlies. If the eddy fluxes were held fixed, the response of zonal winds would be purely barotropic (Robinson 2000). However the vertical shear in the zonal winds also increases somewhat, a response that we attribute

to the reduction in the eddy kinetic energy and poleward heat flux due to the barotropic governor. The poleward shift during the slow adjustment also displays an equivalent barotropic structure outside of the tropics, as expected from the response to a latitudinal displacement of the eddy-driven component of the wind field forced by a shift of the upper level eddy momentum flux convergence (Robinson 2000). The equilibrated response is the consequence of the initial rapid barotropic acceleration at the jet latitude and the following slow poleward jet shift.

[Figure 6 about here.]

Consistent with the surface winds, the poleward movement of the eddy momentum flux convergence (Fig. 5d) occurs primarily during the slow response. The increase in barotropic component of the flow and the reduction in eddy kinetic energy occur before there is a substantial poleward displacement. There is also some reduction in the magnitude of the momentum flux initially, after which there is slow recovery.

Because the eddy energy reduction is so rapid and large, if the barotropic governor were central to the forcing of the poleward shift, we might expect a more rapid response of the zonal mean jet. This suggests that the barotropic governor mechanism, responsible for the eddy energy reduction, may not be directly linked to the poleward displacement.

Given the two-phase character of the adjustment, with slow poleward displacement, we believe that the idealization described in R97, with an initial phase in which the mean flow adjusts in place to the drag, with no change in eddy activity, is still useful, even though there are, in fact, significant changes in eddy amplitude in this phase.

4. The eddy flux cospectra and the critical latitude shift

In order to characterize more fully the wave activity redistribution in the upper troposphere, we plot spectra of the upper tropospheric ($\sigma = 0.275$) momentum flux convergence as a function of latitude and angular phase speed (Randel and Held 1991; Lee 1997; Kim and Lee 2004) in Fig. 7. We utilize angular phase speed rather than phase speed (c), because the former is conserved as a Rossby wave packet propagates meridionally in a zonally symmetric background flow. (In the figure we actually use $c_A = c/\cos\phi$, the angular phase speed multiplied by the radius of the Earth a.) To estimate the spectrum, we divide the model output into 10 periods of length T = 160 days. The resolution in phase speed space, Δc_A, is limited by the time period T and the zonal wavenumber m, $\Delta c_A = a(2\pi/T)/m$. Because of its large Δc_A, we ignore the very small contribution to the flux from $m = 1$ in this plot.

The spectra are primarily confined between two critical latitudes (where $\bar{u}/\cos\phi = c_A$) defined by the time mean flow at this upper tropospheric level, with the faster waves restricted to the regions near, and somewhat equatorward of, the jet maximum. Since Rossby waves prefer to propagate equatorward on the sphere, and tend to break before they reach their linear critical latitudes, most of the wave activity diverging from midlatitudes converges close to, but somewhat poleward of, the subtropical critical latitude.

[Figure 7 about here.]

As the mean drag is reduced from 0.5 day to 1.5 day, the range of eddy angular phase speeds at the latitudes of 20-40° extends from -7∼20 m/s to -5∼30 m/s. The

difference between these two spectra emphasizes the increase in equatorward propagation in waves with angular phase speeds of 10$\sim$30 m/s and the decrease with phase speeds of -7$\sim$10 m/s. The poleward movement of the divergence is especially associated with the faster phase speeds.

This increase of angular phase speed is a plausible consequence of the barotropic increase of extratropical westerly winds (Fig. 6a) that occurs during the fast adjustment. The subtropical zonal winds barely change, partly because they overlie weak surface winds near the transition from easterlies to westerlies, where the effect of the reduction in the mean drag is not strongly felt. The net effect of the increase in phase speed of the dominant eddies and the lack of increase in the subtropical upper level winds, is a poleward shift of the subtropical critical latitude.

More explicitly, assume that the fast response is purely barotropic in the latitudes between the surface westerly wind maximum and the critical latitude for the dominant waves. It is then reasonable to expect the phase speed of the dominant eddies to be modified by an amount equal to the surface wind change at the center of the storm track, located near the center of the surface westerlies (ϕ_w): $\delta c \approx \delta u_s(\phi_w)$. The change in the upper level winds near the critical latitude ϕ_c for these dominant waves, assuming a barotropic response, is $\delta u_s(\phi_c)$. The critical latitude moves poleward provided that $\delta u_s(\phi_w) > \delta u_s(\phi_c)$, or, assuming that these changes in the surface winds are approximately the unperturbed winds times the change in frictional time scale, $u_s(\phi_w) > u_s(\phi_c)$.

To support the speculation described above, we plot the eddy spectral changes in the fast adjustment in Fig. 8. The space-time spectra are calculated by perform-

ing Fourier transforms over days 1-30, averaging among 30 ensemble members, and subtracting the spectra for the control simulation. Due to limitations of the spectral resolution, we show the results only for $m \geq 5$, but these are the dominant waves in the eddy momentum flux. It is seen that there is indeed a phase speed increase in the fast adjustment, and a slight poleward shift in the eddy momentum flux convergence. However, the magnitude of the increase in phase speed is less than half of that in the equilibrated state (note the smaller contour interval in Fig. 8). The implication is that some of the increase in phase speed accompanies the poleward displacement.

The eddy heat flux in the lower troposphere ($\sigma = 0.875$) displays a similar increase in dominant phase speeds and a poleward shift in the equilibrated response (Fig. 7) and a smaller increase in phase speeds in the fast transient response (Fig. 8). Our hypothesis is that this lower level eddy flux displacement is driven by the displacement in the latitude of the upper level disturbance. The underlying mechanism connecting the upper to the lower troposphere can be thought of in several ways. One can argue that baroclinic instability, as traditionally measured by the Eady growth rate in the lower troposphere, is directly modified by zonal winds and associated vertical shears generated by upper level eddy momentum fluxes. Alternatively, one can think of the near surface temperatures as being stirred by upper tropospheric potential vorticity anomalies, and use a diffusive eddy closure argument for the lower level eddy heat fluxes by defining the diffusivity to be proportional to the upper level stream function variance (Held 1999).

[Figure 8 about here.]

While it seems plausible that the shift in phase speeds and the subtropical critical

latitude is related to the displacement of the eddy fluxes, it is not straightforward to make a quantitative connection between the two, given the potentially complicated wave breaking processes in the upper troposphere and their feedback onto the lower tropospheric disturbances. Hartmann and Zuercher (1998) provide some interesting insights on this connection from the nonlinear life cycle point of view. For the case of stronger anticyclonic shear on the equatorward side of the initial jet (corresponding to smaller shear parameter in their paper), the eddy phase speed is faster, implying a more poleward critical latitude. However, the transition from LC2 to LC1, in favor of a poleward jet shift, occurs only at a threshold value, therefore it is unclear in these calculations if the phase speed change and the jet shift are closely connected.

We have also performed life cycle calculations with the control climatological mean winds, varying the barotropic component of the flow within the range of the changes in the mean drag experiments. Only LC1, accompanied by a poleward jet shift from the initial jet latitude, is found for either the most unstable mode ($m = 8$) or the energy containing mode in the control experiment ($m = 5$). Furthermore, the poleward shift is smaller in the case of larger barotropic flow (larger anticyclonic shear in the subtropics). Given the inconclusive character of these life cycle results, we turn instead to a stirred shallow water model of the upper troposphere.

5. A shallow water model of upper troposphere

A simple model is constructed to study the wave activity redistribution and the associated jet shift in the upper troposphere. The notion is to idealize the upper troposphere as one shallow water layer forced by random stirring in the divergence field. Stirring in

the divergence equation is equivalent to specifying a stochastic component in the pressure gradient below the active layer. Models built on similar ideas have been used to study the eddy momentum fluxes and wave-mean flow interaction (Held and Phillips 1990; Delsole 2001; Orlanski 2003; Vallis et al. 2004). Our model configuration is described in detail in the Appendix, and has the following characteristics:

- The model is nonlinear so as to directly simulate wave breaking.
- The upper layer is stirred by specifying a stochastic source to the divergence equation, so that the stirring does not modify the potential vorticity. We believe that this is more physical than directly stirring in the potential vorticity or vorticity field, in that this does not introduce an explicit source in the pseudomomentum conservation equation.
- The stirring has a space-time spectrum centered on a characteristic angular phase speed, and is localized in midlatitudes, with no feedback onto the stirring from the upper layer dynamics. In the calculations described, the stirring amplitude is modest in the sense that there is relatively little inverse cascade of energy.
- There is a lower layer with no eddies but with a zonal mean wind that is assumed to be equal to the eddy momentum flux convergence in the upper layer divided by a surface damping rate; these winds feed back onto the upper tropospheric winds via thermal wind balance. This allows us to separately modify the barotropic shears, by varying the surface damping, and the characteristic phase speed of the stirring.
- The interface between the two layers or, equivalently, the upper layer thickness, is relaxed to a specified radiative equilibrium value.

- The rigid top of the upper layer is given some latitudinal structure, increasing the thickness of the upper layer in the tropics, to assist in generating a plausible control simulation.

Some features of the control simulation with this shallow model are displayed in Fig. 9. This model generated poleward eddy thickness fluxes as well as eddy momentum fluxes that converge in midlatitudes. The equator-to-pole thickness gradient is reduced by the poleward eddy thickness flux and is restored by the relaxation towards radiative equilibrium. (In the absence of the stirring, the model generates a weak tropically confined Hadley cell.) Coherent Rossby wave packets are generated that resemble those in observations (cf. Lee and Held (1993); Chang and Yu (1999)). The lower layer winds balance the eddy momentum flux convergence, and have a reasonable structure and amplitude.

[Figure 9 about here.]

We study the model sensitivity with three independent model parameters: the mean drag on the lower layer flow, τ_f, the angular speed characterizing the stirring, $\bar{u}_A$, and the stirring amplitude A (Fig. 10).

As the mean drag is reduced, the lower layer westerlies increase proportionally and feedback on the upper layer jet by construction, but no poleward displacement is observed. There is little effect on eddy kinetic energy of this increase in meridional shears in the shallow water model, consistent with the view that the way that barotropic governor reduces eddy amplitudes, is not simply by increasing the efficiency of barotropic conversion, but through the baroclinic production that involves interfering with the coupling between upper and lower level disturbances.

As the stirring amplitude increases, eddy amplitudes naturally increase, and the surface westerlies and the jet are displaced polewards. The stronger stirring in the shallow water model leads to more zonal wind deceleration in the subtropics, so the shift in zonal winds is similar to what occurs in the LC1 life cycle. We have not forced the model strongly enough, or at small enough scales, to enter the regime described in Orlanski (2003) in which cyclonic wave breaking becomes prevalent. Inspection of the idealized GCM also suggests that this is the case in that model as well. We believe that it is easier to enter the cyclonic regime when modelling zonally asymmetric storm tracks with much stronger local jets.

As the eddies increase in strength, the stronger anticyclonic breaking in the subtropics moves the jet polewards. Since eddy amplitudes decrease as the mean drag is reduced in the idealized GCM, we cannot explain the poleward shift in this way. The shallow water model results do not provide any evidence that either the increase in meridional shears or the decreasing eddy energies are directly responsible for the jet shift.

[Figure 10 about here.]

In contrast, the jet shifts poleward in the shallow water model when the phase speeds in the stirring are increased, with qualitative resemblance to the behavior of the idealized GCM when the mean drag is reduced. The shallow water model eddy momentum flux convergence is plotted as a function of latitude and angular phase speed in Fig. 11 for two experiments with different stirring phase speeds. The spectral shift is comparable in structure to that in the GCM mean drag experiments (Fig. 7), with a poleward shift in the eddy momentum fluxes accompanying the increase in

phase speed.

[Figure 11 about here.]

The size of the jet shift in this shallow water model is less than that in the mean drag runs with the idealized GCM. In Fig. 2, the jet shifts poleward 10 degrees as the barotropic wind increases by 10 m/s. But in Fig. 10, the jet shifts 10 degrees as $\bar{u}_A$ increases by 20 m/s. In addition, as we have just seen, a reduction in eddy energy as occurs in the idealized GCM should further reduce the amplitude of the shift. It is possible that this deficiency is due to problems in representing the upper troposphere as a single layer. However, we believe that the main deficiency in this model is that as the jet moves poleward, the stirring emanating from the lower troposphere should also move poleward, following the upper level eddy activity, as implied by the poleward shift of the lower tropospheric heat flux in the GCM (Fig. 7). The shallow water model, therefore, excludes an important positive feedback that amplifies the jet response to reduced drag in the full model.

Despite these limitations, we suspect that this shallow water model provides a useful approach towards understanding the jet shift. The model can be further elaborated in several ways, as, for example, by studying in greater detail the wave breaking in the shallow water model as the parameters in this model are varied, or by studying alternative ways of connecting the statistics of the stirring to the statistics of the upper level solution.

6. Conclusion and Discussion

The sensitivity to surface friction of the latitude of the surface westerlies and the associated eddy-driven mid-latitude jet is studied in an idealized dry GCM. This latitude is mainly determined by the friction on the zonal mean flow rather than the friction on the eddies. The relatively small variation in eddy kinetic energy as the total drag is changed is the result of two competing large effects: a direct increase in eddy energy as the eddy drag is reduced; and an indirect reduction in eddy energy through the effect of meridional shears on baroclinic instability (the barotropic governor) as the mean drag is reduced. We focus on the effects of mean drag in this paper. Motivated by examination of the space-time spectra of the eddies in the GCM, we construct a shallow water model to study the reaction of the upper tropospheric dynamics to an increase in the eastward phase speed in the dominant midlatitude eddies. The shallow water calculations support the view that this increase in phase speed is a key ingredient in the poleward shift of the surface westerlies.

Our study suggests that the response of the atmosphere to the change of surface friction on the mean flow can be understood as follows:

1 As the surface drag is reduced, the zonal wind acceleration is barotropic and proportional to the surface wind in the extratropics. Meanwhile, the baroclinic eddies are weakened by the increased barotropic meridional shear, but neither the weakening eddies nor the increased meridional shears are directly implicated in the poleward shift.

2 The increase in the strength of the westerlies in the extratropics leads to faster eddy phase speeds, while the subtropical zonal winds barely change. Hence, the

critical latitude for these eddies is displaced poleward.

3 The dynamics of the wave breaking in the upper troposphere, in the presence of this poleward shift in critical latitude, shifts the eddy momentum fluxes polewards, driving a poleward shift in the surface zonal winds and the eddy driven jet. This is particularly supported by the shallow water model results.

4 Eddy heat fluxes, and the associated upward EP fluxes tend to follow this upper level eddy activity. This shift in the baroclinic eddy production provides some positive feedback on the upper level shift.

Even when one focuses on the effects of mean drag, there are evidently competing tendencies that must be considered in analyzing the resulting climatic responses. The effects of the phase speed shift may be compensated, in part, by the effects of the reduction in the eddy energy due to the barotropic governor. When the strength of the stirring is reduced in the shallow water model, there is an equatorward displacement of zonal winds (we see a similiar effect in nonlinear life cycle simulations not shown here). The critical latitude shift is apparently dominant over the effect of decreasing eddy energy in our mean drag experiments. We also note that to the extent that the atmosphere is at times in a cyclonic breaking regime due to high eddy amplitude and small eddy length scale as described in Orlanski (2003), a reduction in eddy energy could have the opposite effect of generating poleward movement.

We have confirmed that similar wind shifts occur in the idealized GCM when the change in mean drag is replaced by a prescribed torque approximating the change in mean drag in the GCM experiments. The interactive character of the drag and the zonal mean is not essential for the climatic response, consistent with the dynamics

outlined above. It is then natural to inquire as to the dependence of the response on the structure of the imposed torque. We hope to address this problem in the future.

The tropospheric eddy phase-speed mechanism is potentially relevant to many other cases in which the surface westerlies shift in latitude in response to some perturbation, since the strength of the zonal flow that controls the eddy phase speed can be affected by a variety of factors other than surface friction. As an example, tropospheric zonal winds can be modified by a stratospheric zonal torque due to planetary or gravity waves via the "downward control" mechanism (Haynes et al. 1991; Song and Robinson 2004). The responses of zonal winds and EP fluxes in the troposphere to the idealized stratospheric perturbation in Polvani and Kushner (2002), are qualitatively very similar to the effects of surface drag. Changes in tropospheric phase speeds may play a role in this stratosphere-troposphere coupling context as well. They may also be relevant to the unforced annular mode variability of the tropospheric zonal winds.

The westerlies at the tropopause level in midlatitudes can also be increased by warming the tropical upper troposphere, as in global warming simulations, or by cooling the polar stratosphere, as in the response to the ozone hole. The increased lower stratospheric and upper tropspheric mean winds may be sufficient to increase eddy phase speeds so as to shift the circulation polewards.

APPENDIX

A shallow water model of the upper troposphere

For simplicity, we consider two layers of an incompressible fluid with densities ρ_1, ρ_2 ($\rho_1 < \rho_2$) rather than two isentropic layers of a compressible ideal gas. The thicknesses of the two layers, multiplied by the reduced gravity $g^* \equiv g(\rho_2 - \rho_1)/\rho_1$ for convenience, are denoted by $\mathcal{H}_1$ and $\mathcal{H}_2$. We allow ourselves the freedom of specifying a latitudinal dependence in the height of the upper boundary at z_{top} and also set $\mathcal{H}_{top} = g^* z_{top}$. The lower boundary is flat. Setting $S \equiv p_s/\rho_1$, where p_s is the surface pressure, the horizontal pressure gradient in the upper layer is

$$-\frac{1}{\rho_1}\nabla p_1 = -\nabla(S - \mathcal{H}_2) = -\nabla(S - (\mathcal{H}_{top} - \mathcal{H}_1)) \tag{5}$$

The pressure gradient in the lower layer is also proportional to ∇S, and this term is responsible for the interaction between the two layers.

We use Newtonian relaxation of the interface with strength κ_T, linear damping of momentum meant to represent vertical mixing with strength κ_M, and subgrid hyperdiffusion (∇^8) proportional to κ_v. The equations for the upper layer thickness, vorticity, and divergence are

$$\frac{\partial \mathcal{H}_1}{\partial t} = -\nabla \cdot (\mathbf{v}_1 \mathcal{H}_1) - \kappa_T(\mathcal{H}_1 - \mathcal{H}_{1eq}) - \kappa_v \nabla^8 \mathcal{H}_1 \tag{6}$$

$$\frac{\partial \zeta_1}{\partial t} = -\nabla \cdot (\mathbf{v}_1(f + \zeta_1)) + F_{\zeta_1} - \kappa_M \zeta_1 - \kappa_v \nabla^8 \zeta_1 \tag{7}$$

$$\frac{\partial D_1}{\partial t} = -\nabla \cdot ((f + \zeta_1)\mathbf{k} \times \mathbf{v}_1) - \nabla^2\left(\frac{u_1^2 + v_1^2}{2} + S + \mathcal{H}_1 - \mathcal{H}_{top}\right) + F_{D_1} - \kappa_M D_1 - \kappa_v \nabla^8 D_1. \tag{8}$$

$\mathcal{H}_{1eq}$ is the equilibrium thickness for the upper layer. Since the shape of the upper boundary is fixed in time, one can equivalently think of relaxing the interface to its radiative equilibrium value. The forms chosen for $\mathcal{H}_{1eq}$ and $\mathcal{H}_{top}$ are

$$\mathcal{H}_{1eq} = \mathcal{H}_m + \Delta\mathcal{H}(\cos^6\phi - 0.5) \tag{9}$$

$$\mathcal{H}_{top} = 2\mathcal{H}_m + \Delta\mathcal{H}(\cos^6\phi - \cos^3\phi) \tag{10}$$

The term (F_{ζ_1}, F_{D_1}) represents the vertical momentum fluxes associated with the diabatic mass fluxes, and is only applied to the zonal mean flow for simplicity. It takes the following form in the momentum equations, which can be thought of as the simplest upstream finite-differencing of vertical advection (Shell and Held 2004).

$$F_{\bar{\mathbf{v}}_1} = -(\bar{\mathbf{v}}_1 - \bar{\mathbf{v}}_2)\max(Q, 0) \tag{11}$$

where $Q = -\kappa_T(\bar{\mathcal{H}}_1 - \mathcal{H}_{1eq})/\bar{\mathcal{H}}_1$. This term, and the vertical mixing, are included to prevent excessive upper tropospheric easterlies at the equator. They have little direct effect on the solution in midlatitudes.

The surface pressure S has two parts, a zonal mean component that evolves in time to balance a zonal mean low level wind, and a stochastic eddy part that drives the eddy field. The zonal mean surface pressure is assumed to be in geostrophic balance with the zonal mean lower layer flow; this lower layer flow in turn is determined by predicting a barotropic zonal mean flow $\bar{u}_{bt}$ driven by the eddy momentum fluxes in

the upper layer:

$$\frac{\partial \bar{u}_{bt}}{\partial t} = -\frac{\bar{\mathcal{H}}_1}{\mathcal{H}_{top}} \frac{1}{a\cos^2\phi} \frac{\partial(\overline{v_1' u_1'}\cos^2\phi)}{\partial\phi} - \frac{\bar{\mathcal{H}}_2}{\mathcal{H}_{top}} \kappa_f^* \bar{u}_2 - \kappa_v \nabla^8 \bar{u}_{bt} \quad (12)$$

$$\frac{1}{a}\frac{\partial \bar{S}}{\partial\phi} = -f\bar{u}_2, \quad \bar{u}_2 = \frac{1}{\bar{\mathcal{H}}_2}(\mathcal{H}_{top}\bar{u}_{bt} - \bar{\mathcal{H}}_1\bar{u}_1) \quad (13)$$

In Eq. (12), the surface drag coefficient is set to be a function of layer thicknesses $\kappa_f^* = (\bar{\mathcal{H}}_1/\bar{\mathcal{H}}_2)\kappa_f$, and thus, in the steady state,

$$-\frac{1}{a\cos^2\phi}\frac{\partial(<\overline{v_1' u_1'}>\cos^2\phi)}{\partial\phi} = \kappa_f <\bar{u}_2> \quad (14)$$

where $<>$ denotes the time average. By combining Eq. (13) with the geostrophic balance in the upper layer, we can obtain the thermal wind relationship in this shallow water model.

$$f(\bar{u}_1 - \bar{u}_2) = \frac{1}{a}\frac{\partial\bar{\mathcal{H}}_2}{\partial\phi} \quad (15)$$

The eddy surface pressure S' is assumed to be independent of the upper layer flow, and is generated by a stochastic process,

$$\frac{\partial\nabla^2 S'}{\partial t} = -\frac{\bar{u}_A}{a}\frac{\partial\nabla^2 S'}{\partial\lambda} - \frac{2\Omega}{a^2}\frac{\partial S'}{\partial\lambda} - r_s\nabla^2 S' + \sum_{m,l}\tilde{\mathcal{E}}_{ml}(t)Y_{ml}(\lambda,\phi) \quad (16)$$

Here $\bar{u}_A$ is the prescribed angular speed, $r_s = 1/\tau_s$ is a frictional damping rate, $Y_{ml}(\lambda,\phi)$ is the spherical harmonic function with the zonal wavenumber m and total wavenumber l, and $\tilde{\mathcal{E}}_{ml}(t)$ is a stochastic forcing (where tilde denotes a complex num-

ber). We force the model only within a prescribed range of wavenumbers, and then localize the forcing in midlatitudes by multiplying by a gaussian function in latitude, $G(\phi_0, \phi_w)$ (where ϕ_0 is the maximum latitude, and ϕ_w is the meridional half-width).

$$\sum_{m,l} \tilde{\mathcal{E}}_{ml}(t) Y_{ml}(\lambda, \phi) = AG(\phi_0, \phi_w) \sum_{m,l} \tilde{W}_{ml}(t) Y_{ml}(\lambda, \phi) \tag{17}$$

where $\tilde{W}_{ml}(t)$ is generated by a gaussian random variable with unit variance, decorrelated in time and wavenumbers, and A is a parameter with which we control the amplitude of the stirring.

The equation (16) is discretized as,

$$\begin{aligned} \frac{\nabla^2 S'(i+1) - \nabla^2 S'(i-1)}{2\Delta t} &= -\frac{\bar{u}_A}{a} \frac{\partial \nabla^2 S'(i)}{\partial \lambda} - \frac{2\Omega}{a^2} \frac{\partial S'(i)}{\partial \lambda} - r_s \nabla^2 S'(i) \\ &+ (2\Delta t)^{-1/2} \sum_{m,l} \tilde{\mathcal{E}}_{ml}(i) Y_{ml}(\lambda, \phi) \end{aligned} \tag{18}$$

Where i denotes the ith time step, the factor $(2\Delta t)^{-1/2}$ is included to maintain the same variance as the time step is changed.

In spherical harmonic space, Eq. (16) can be written as follows,

$$\frac{\partial \tilde{S}_{ml}(t)}{\partial t} = -(i\omega_R + r_s)\tilde{S}_{ml} - \frac{a^2}{l(l+1)} \tilde{\mathcal{E}}_{ml}(t), \quad \omega_R = m\frac{\bar{u}_A}{a} - m\frac{2\Omega}{l(l+1)} \tag{19}$$

Thus, we obtain the frequency spectrum of the eddy surface pressure,

$$|\tilde{S}_{ml}(\omega)|^2 = \frac{a^4}{l^2(l+1)^2} \frac{|\tilde{\mathcal{E}}_{ml}(\omega)|^2}{(\omega - \omega_R)^2 + r_s^2}, \tag{20}$$

Here $|\tilde{\mathcal{E}}_{ml}(\omega)|^2$ is the variance of the white noise process. $|\tilde{S}_{ml}(\omega)|^2$ is reddened by the frictional damping r_s and is maximum at the frequency ω_R.

We adopt the following control values for this model, approximately following Held and Phillips (1990) and Vallis et al. (2004).

$$\kappa_T^{-1} = 10 \text{ days}, \quad \kappa_M^{-1} = 100 \text{ days}, \quad \kappa_f^{-1} = 5 \text{ days}, \quad \kappa_s^{-1} = 2 \text{ days}$$

$$\mathcal{H}_m = 0.7 \times 10^4 m^2 s^{-2}, \quad \Delta\mathcal{H} = 1.0 \times 10^4 m^2 s^{-2}$$

$$A_c(2\Delta t)^{-1/2} = 1.5 \times 10^{-14}, \quad \Delta t = 1200 \text{ seconds}$$

$$\bar{u}_A = 15 m/s, \quad \phi_0 = 45^o, \quad \phi_w = 15^o, \quad 5 \leq m \leq l \leq 12 \tag{21}$$

The shallow water model is run at the same resolution and hyperdiffusion, and is sampled and averaged over the same time periods as is the idealized GCM.

References

Chang, E. K. M. and D. B. Yu, 1999: Characteristics of wave packets in the upper troposphere. Part I: Northern hemisphere winter. *J. Atmos. Sci.*, **56**, 1708–1728.

Delsole, T., 2001: A simple model for transient eddy momentum fluxes in the upper troposphere. *J. Atmos. Sci.*, **58**, 3019–3035.

— 2004: Stochastic models of quasigeostrophic turbulence. *Surveys in Geophys*, **25**, 107–149.

Frierson, D. M. W., I. M. Held, and P. Zurita-Gator, 2006: A gray-radiation aquaplanet moist GCM. Part I: Static stability and eddy scales. *J. Atmos. Sci.*, In press.

Fyfe, J., G. Boer, and G. Flato, 1999: The Arctic and Antarctic Oscillations and their projected changes under global warming. *Geophys. Res. Lett.*, **26**, 1601–1604.

Gillett, N. P. and D. W. J. Thompson, 2003: Simulation of recent southern hemisphere climate change. *Science*, **302**, 273–275.

Haigh, J. D., M. Blackburn, and R. Day, 2005: The response of tropospheric circulation to perturbations in lower-stratospheric temperature. *J. Climate*, **18**, 3672–3685.

Hartmann, D. L. and P. Zuercher, 1998: Response of baroclinic life cycles to barotropic shear. *J. Atmos. Sci.*, **55**, 297–313.

Haynes, P. H., C. J. Marks, M. E. McIntyre, T. G. Shepherd, and K. P. Shine, 1991: On the ”downward control” of extratropical diabatic circulations by eddy-induced mean zonal forces. *J. Atmos. Sci.*, **48**, 651–678.

Held, I. M., 1999: The macroturbulence of the troposphere. *Tellus*, **51A-B**, 59–70.

Held, I. M. and P. J. Phillips, 1990: A barotropic model of the interaction between the Hadley cell and a Rossby wave. *J. Atmos. Sci.*, **47**, 856–869.

Held, I. M. and M. J. Suarez, 1994: A proposal for the intercomparison of the dynamical cores of atmospheric general circulation models. *Bull. Amer. Meteor. Soc.*, **75**, 1825–1830.

James, I. N., 1987: Suppression of baroclinic instability in horizontally sheared flows. *J. Atmos. Sci.*, **44**, 3710–3720.

Kim, H. and S. Lee, 2004: The wave-zonal mean flow interaction in the southern hemisphere. *J. Atmos. Sci.*, **61**, 1055–1067.

Kushner, P. J., I. M. Held, and T. L. Delworth, 2001: Southern hemisphere atmospheric circulation response to global warming. *J. Climate*, **14**, 2238–2249.

Kushner, P. J. and L. M. Polvani, 2004: Stratosphere-troposphere coupling in a relatively simple AGCM: The role of eddies. *J. Climate*, **17**, 629–639.

Lee, S., 1997: Maintenance of multiple jets in a baroclinic flow. *J. Atmos. Sci.*, **54**, 1726–1738.

— 2005: Baroclinic multiple zonal jets on the sphere. *J. Atmos. Sci.*, **62**, 2484–2498.

Lee, S. and I. M. Held, 1993: Baroclinic wave packets in models and observations. *J. Atmos. Sci.*, **50**, 1413–1428.

Miller, R. L., G. A. Schmidt, and D. T. Shindell, 2006: Forced variations of annular modes in the 20th century IPCC AR4 simulations. *J. Geophys. Res.*, in press.

Orlanski, I., 2003: Bifurcation in eddy life cycles: Implications for storm track variability. *J. Atmos. Sci.*, **60**, 993–1023.

Panetta, R. L., 1993: Zonal jets in wide baroclinically unstable regions: Persistence and scale selection. *J. Atmos. Sci.*, **50**, 2073–2106.

Polvani, L. M. and P. J. Kushner, 2002: Tropospheric response to stratospheric perturbations in a relatively simple general circulation model. *Geophys. Res. Lett.*, **29**, 1114.

Randel, W. J. and I. M. Held, 1991: Phase speed spectra of transient eddy fluxes and critical layer absorption. *J. Atmos. Sci.*, **48**, 688–697.

Rind, D., J. Perlwitz, and P. Lonergan, 2005: AO/NAO response to climates change: 1. Respective influences of stratospheric and tropospheric climate changes. *J. Geophys. Res.*, **110**, D12107, doi:10.1029/2004JD005103.

Robinson, W. A., 1997: Dissipation dependence of the jet latitude. *J. Climate*, **10**, 176–182.

— 2000: A baroclinic mechanism for the eddy feedback on the zonal index. *J. Atmos. Sci.*, **57**, 415–422.

Russell, J. L., A. Gnanadesikan, and J. R. Toggweiller, 2006: Impact of westerly wind position on the circulation of the southern ocean. *J. Climate*, submitted.

Shell, K. M. and I. M. Held, 2004: Abrupt transition to strong superrotation in an axisymmetric model of the upper troposphere. *J. Atmos. Sci.*, **61**, 2928–2935.

Simmons, A. J. and B. J. Hoskins, 1980: Barotropic influences on the growth and decay of nonlinear baroclinic waves. *J. Atmos. Sci.*, **37**, 1679–1684.

Son, S. W. and S. Lee, 2005: The response of westerly jets to thermal driving in a primitive equation model. *J. Atmos. Sci.*, **62**, 3741–3757.

Song, Y. and W. A. Robinson, 2004: Dynamical mechanisms for stratospheric influences on the troposphere. *J. Atmos. Sci.*, **61**, 1711–1725.

Stephenson, D. B., 1994: The northern hemisphere tropospheric response to changes in the gravity-wave drag scheme in a perpetual January GCM. *Quart. J. Roy. Meteor. Soc.*, **120**, 699–712.

Thompson, D. W. J. and S. Solomon, 2002: Interpretation of recent southern hemisphere climate change. *Science*, **296**, 895–899.

Thorncroft, C. D., B. J. Hoskins, and M. E. McIntyre, 1993: Two paradigms of baroclinic wave life-cycle behaviour. *Quart. J. Roy. Meteor. Soc.*, **119**, 17–55.

Vallis, G. K., E. P. Gerber, P. J. Kushner, and B. A. Cash, 2004: A mechanism and simple dynamical model of the North Atlantic Oscillation and Annular Modes. *J. Atmos. Sci.*, **61**, 264–280.

Williams, G. P., 2006: Circulation sensitivity to tropopause height. *J. Atmos. Sci.*, **63**, 1954–1961.

List of Figures

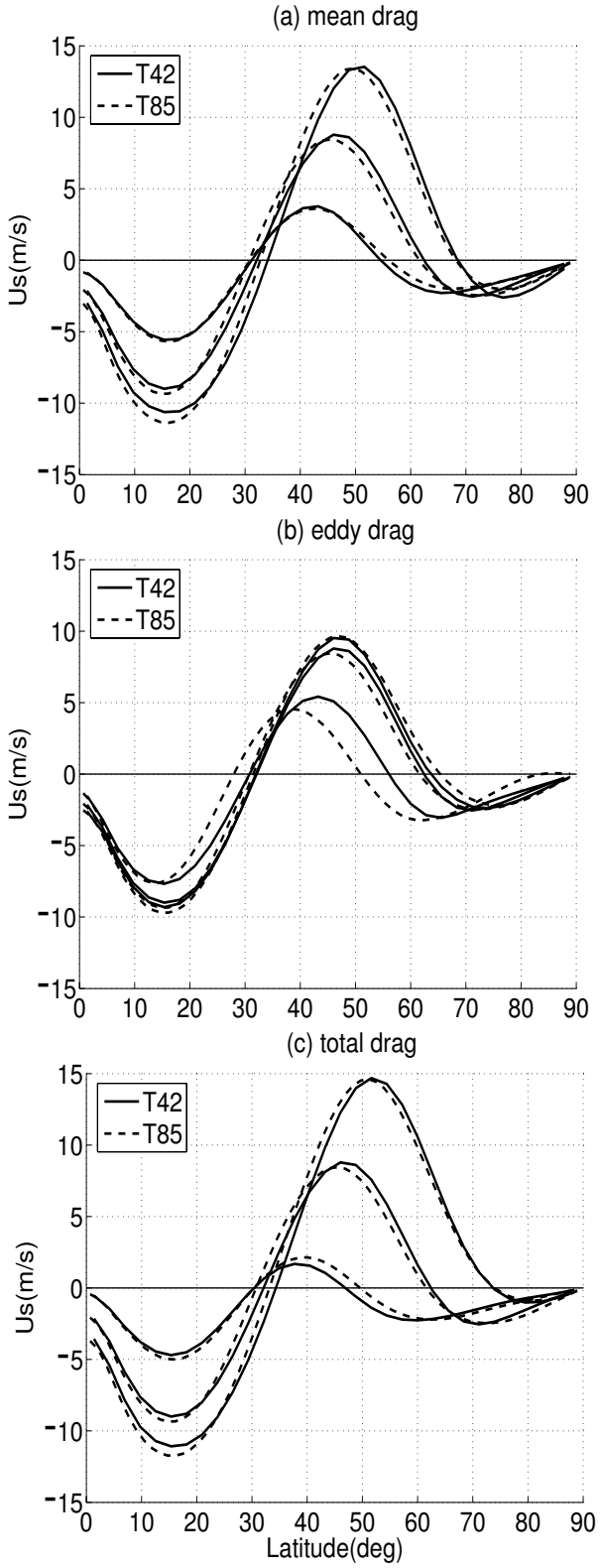

Figure 1: The time and zonally averaged surface winds ($\sigma = 0.975$) as a function of (a) mean drag, (b) eddy drag, (c) total drag at T42 and T85 resolutions. The mean/eddy/total frictional damping times are 0.5, 1.0 and 1.5 day. As the damping time increases (surface friction decreases), both the extratropical westerlies and tropical easterlies are intensified, and the extratropical westerlies are displaced poleward.

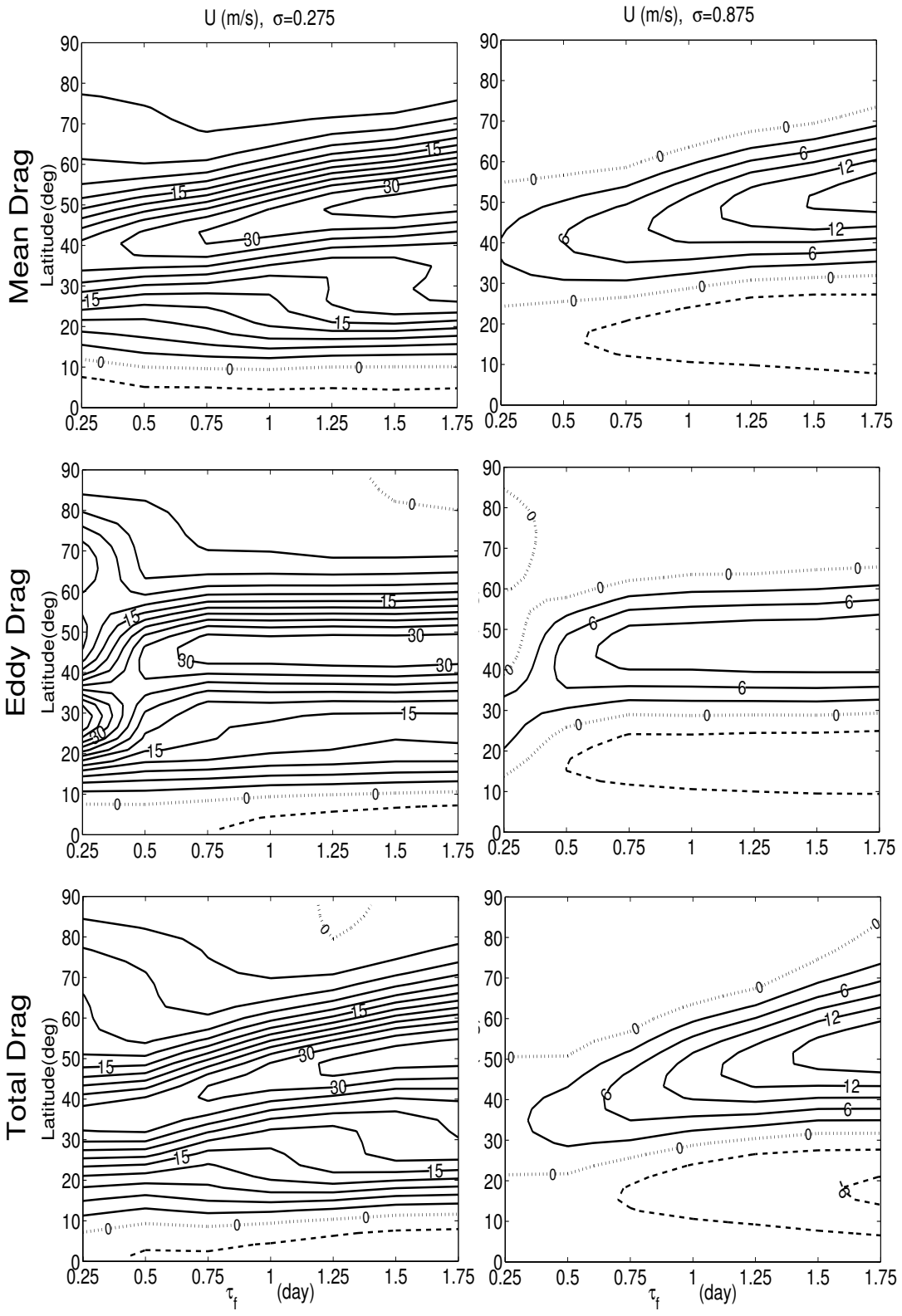

Figure 2: The time and zonally averaged zonal winds at σ=0.275 (Left) and σ=0.875 (Right) as a function of mean drag (Top), eddy drag (Middle) and total drag (Bottom). The contour interval is 3 m/s.

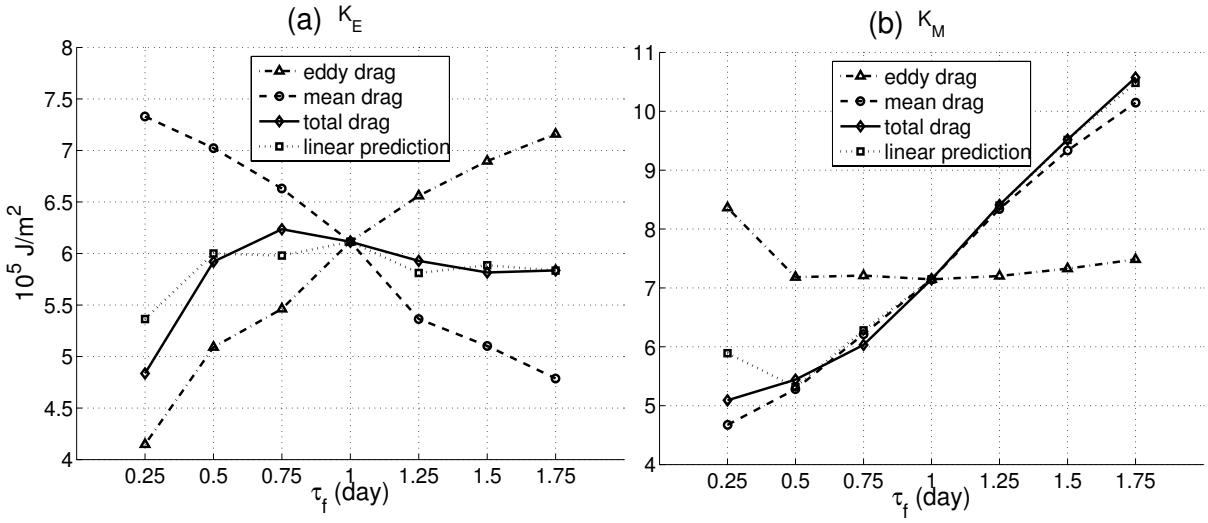

Figure 3: The time and globally averaged (a) eddy kinetic energy and (b) zonal mean kinetic energy as a function of eddy drag, mean drag, total drag, and the linear decomposition. The linear prediction is described in the text.

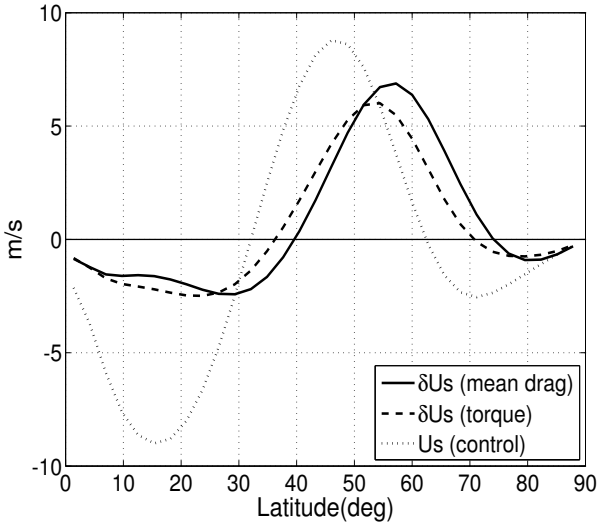

Figure 4: The time and zonally averaged surface wind (σ=0.975) response to the constant torque described in the text using the damping time change from 1.0 to 1.5 day, compared with the surface wind change as the mean drag is reduced from 1.0 to 1.5 day. The torque is proportional to the time and zonal mean surface wind in the control run (dotted).

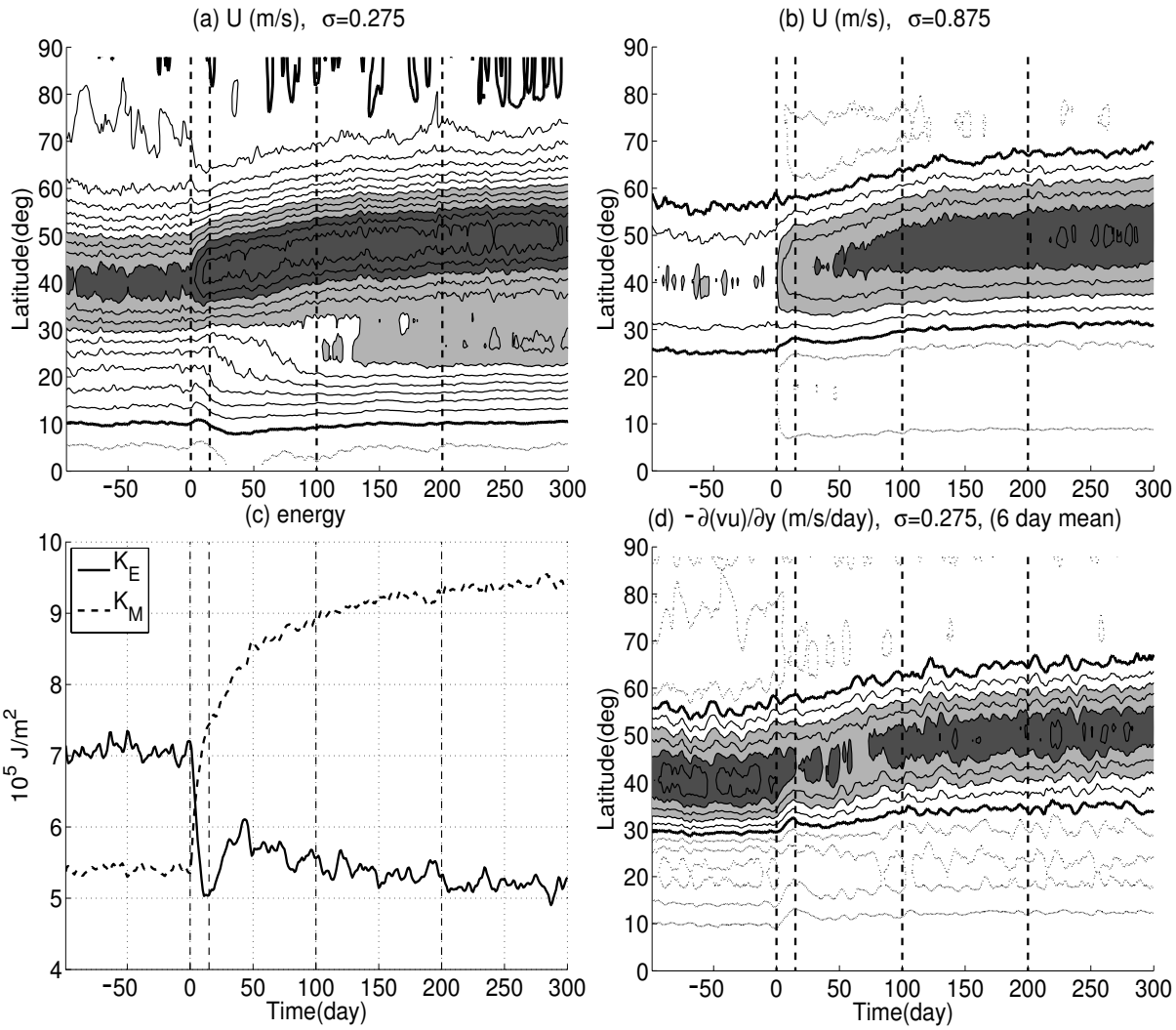

Figure 5: The ensemble means of the transient response: zonal mean zonal winds at (a) σ=0.275 and (b) σ=0.875, (c) global mean energies, and (d) zonal mean eddy momentum flux convergence at σ=0.275. The mean damping time increases from 0.5 to 1.5 day on day 0. The second vertical dashed line indicates day 15. In (a), (b) and (d), the solid (dotted) contours denote positive (negative) values, and thick solid contours denote zeros. The contour interval is 3 m/s for (a) and (b), 1 m/s/day for (d). The figures are plotted using daily data, except for (d) which is smoothed by a 6 day running mean.

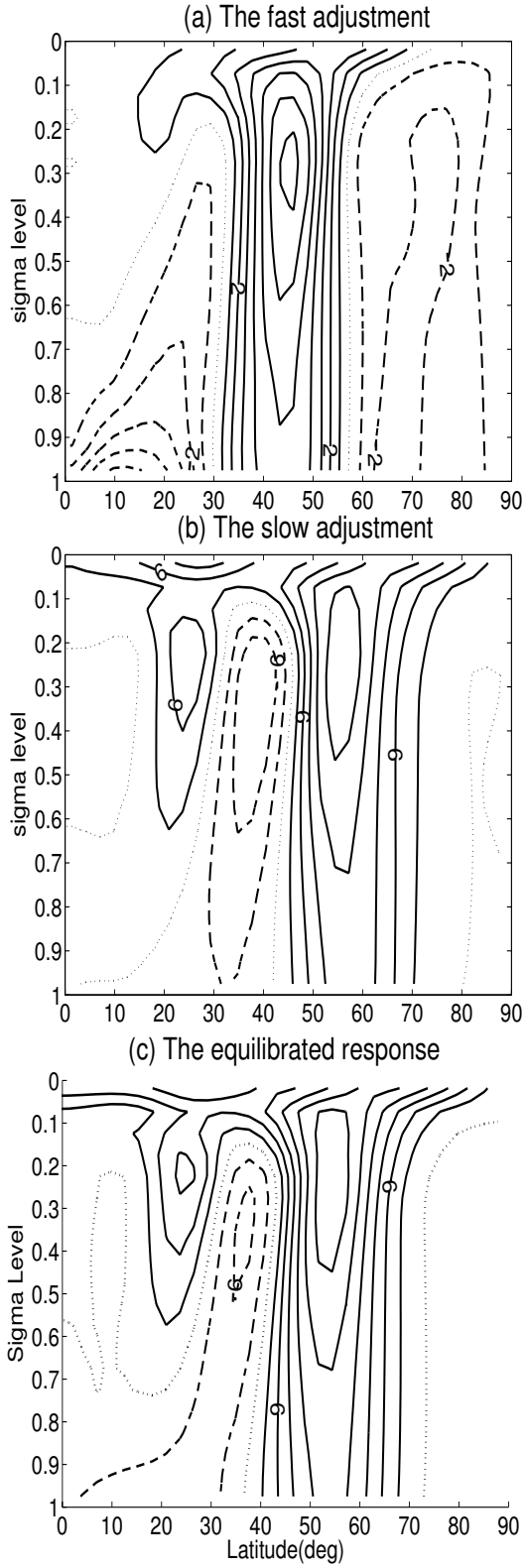

Figure 6: The vertical structure of zonal wind changes during (a) the fast adjustment (days 0-15) and (b) the slow adjustment (days 15-300) in the transient response as in Fig. 5, in comparison with (c) the equilibrated response (1.5 day drag minus 0.5 day drag). The contour intervals are 1 m/s for (a), 3 m/s for (b) and (c).

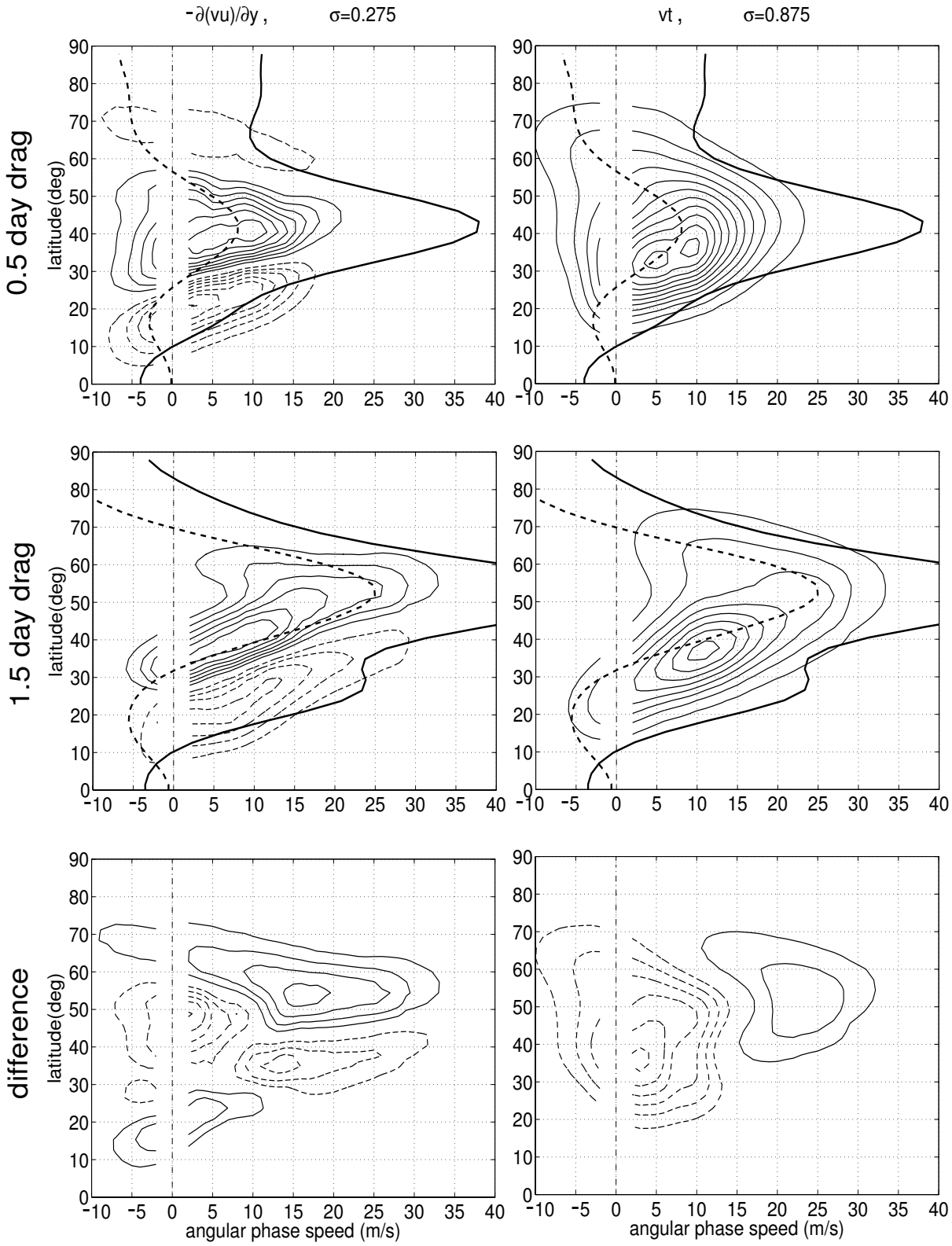

Figure 7: The eddy momentum flux convergence spectra at σ=0.275 (Left) and eddy heat flux spectra at σ=0.875 (Right) for the 0.5 day drag (Top), 1.5 day drag (Middle), the difference (1.5 day drag minus 0.5 day drag) (Bottom) as a function of angular phase speed and latitude. The thick lines are the time and zonally averaged angular velocities at σ=0.275 (solid) and at σ=0.875 (dashed). The contour interval is 0.015 m/s/day for eddy momentum flux convergence, 0.05 Km/s for eddy heat flux, and zero lines are omitted.

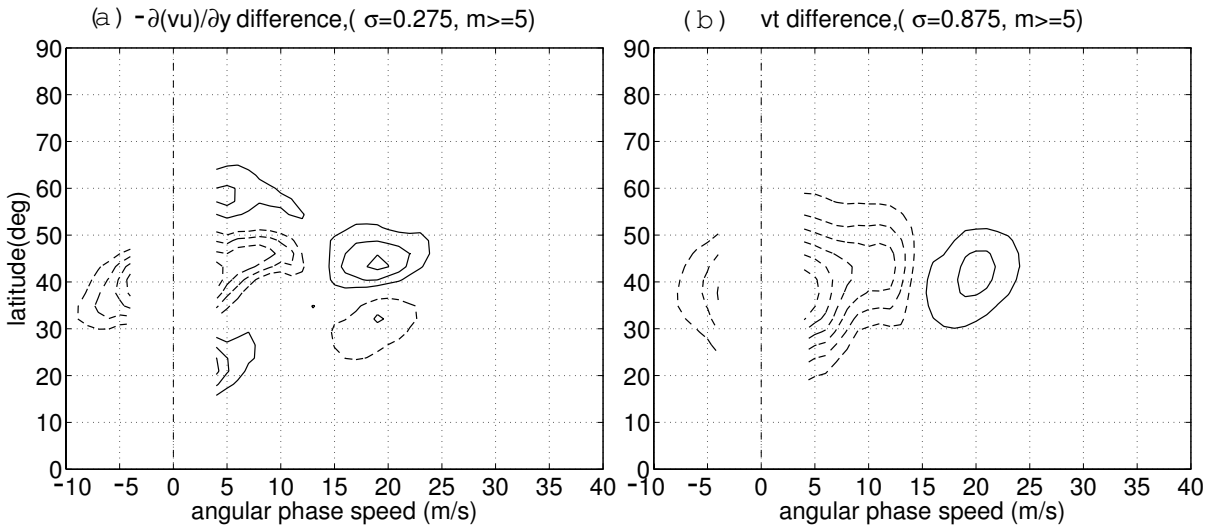

Figure 8: As for Fig. 7, but for the difference of the ensemble mean (a) eddy momentum flux convergence spectra at σ=0.275 and (b) eddy heat flux spectra at $\sigma = 0.875$ in the transient response (days 1$\sim$30 minus the control, where the spectra are calculated by performing Fourier transforms over 30-day periods, and averaging among 30 ensemble members). The spectra only consist of zonal wavenumbers $m \geq 5$. The contour interval is 0.0075 m/s/day for eddy momentum flux convergence, 0.025 Km/s for eddy heat flux.

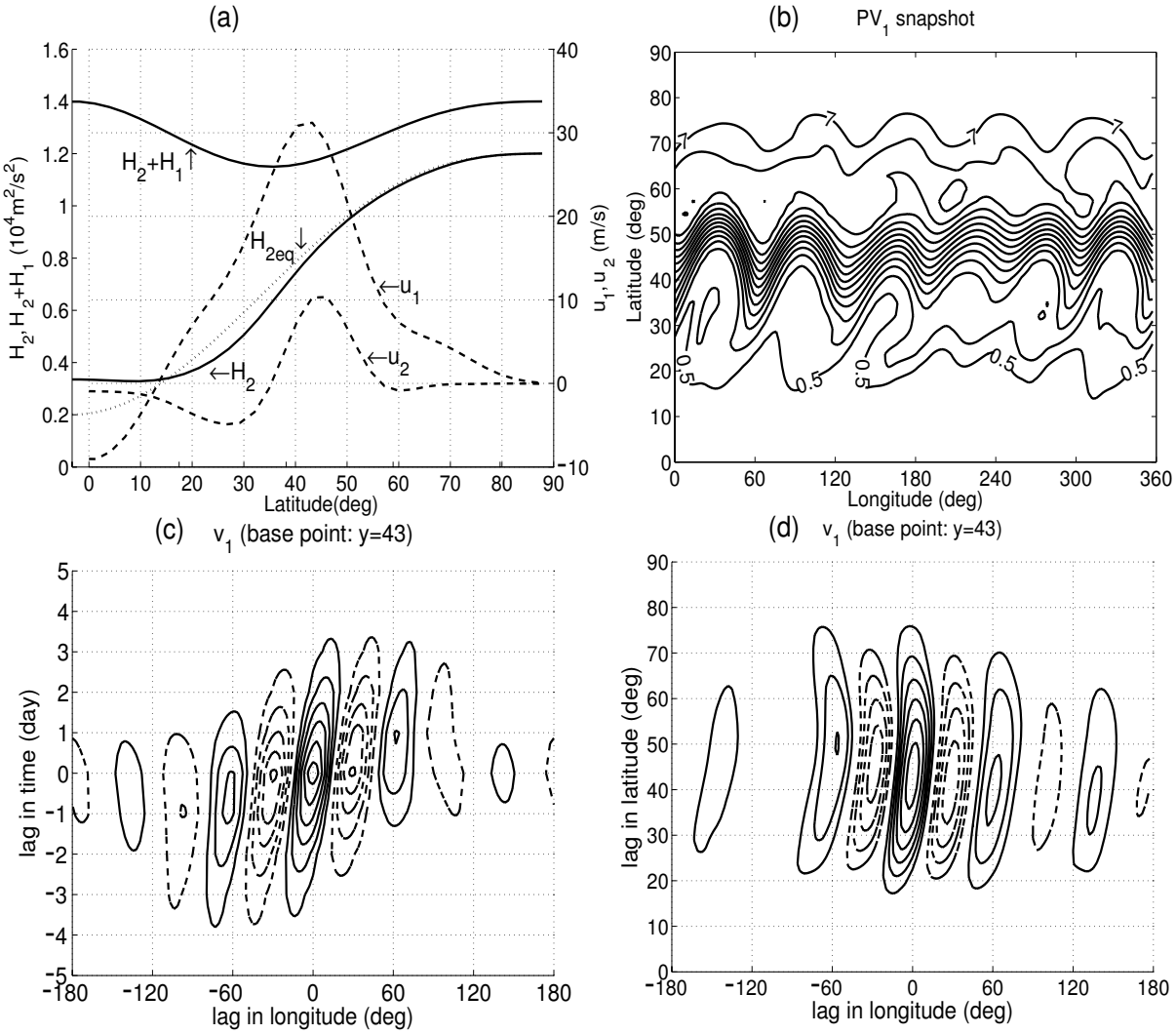

Figure 9: The characteristics of the control experiment in the shallow water model: (a) the time and zonally averaged zonal winds and thicknesses; (b) a potential vorticity snapshot; the lag correlation for the meridional wind at 43° in (c) time and longitude, and (d) latitude and longitude. The contour intervals are $0.5 \times 10^{-8} m^{-2} s$ for (b), 0.15 for (c) and (d).

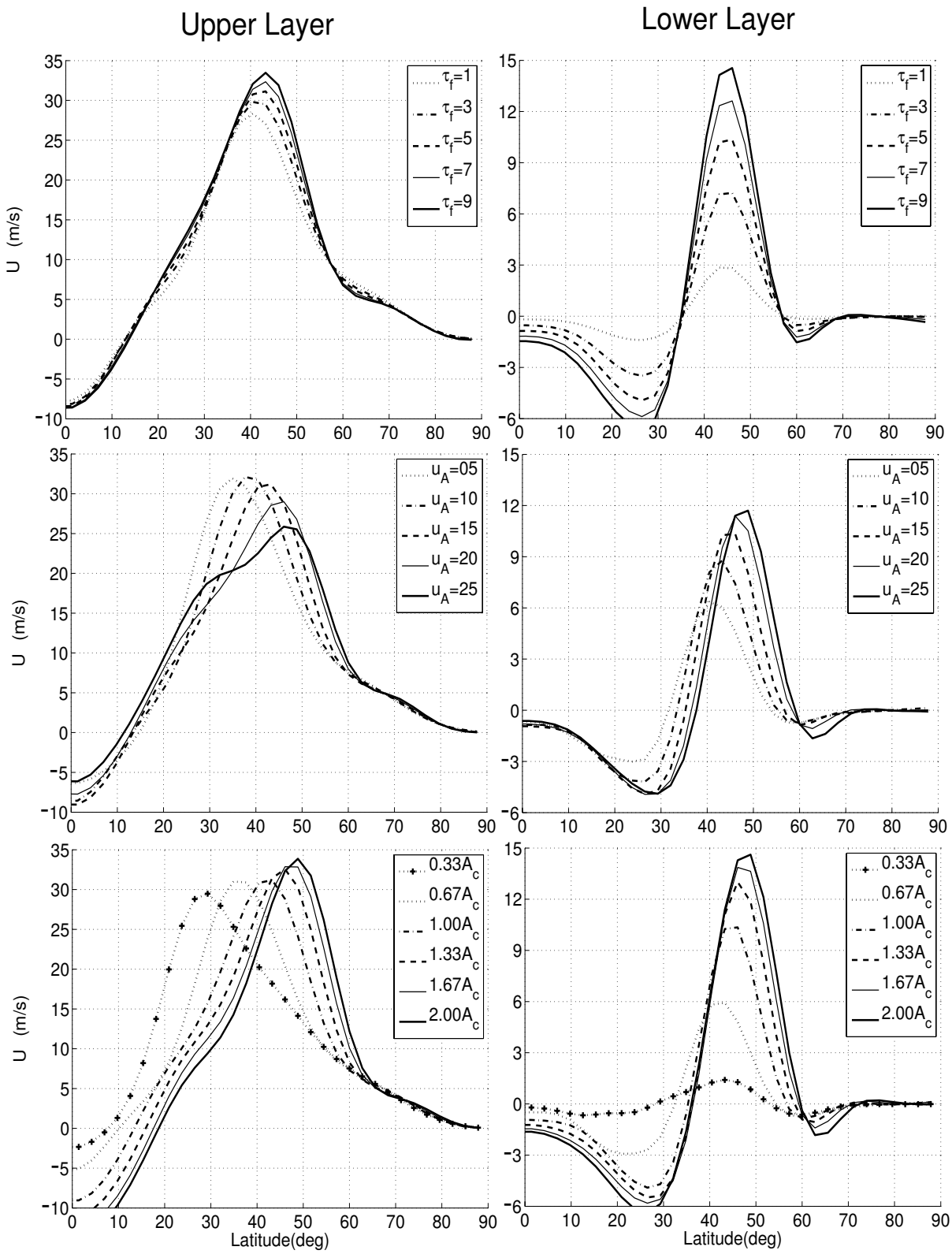

Figure 10: The parameter sensitivity study for the shallow water model: the time and zonally averaged zonal winds in the upper layer (Left) and lower layer (Right) as a function of the mean surface drag (Top), the prescribed angular speed (Middle) and the stirring amplitude (Bottom).

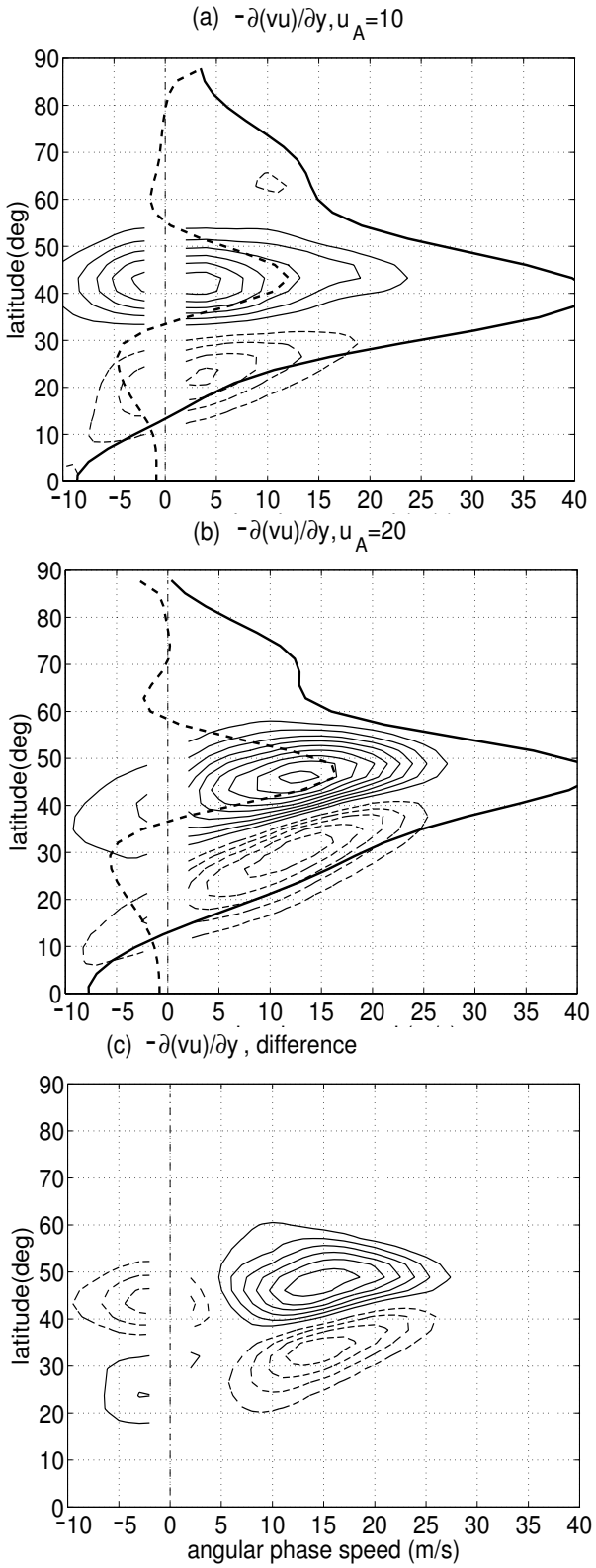

Figure 11: As in Fig. 7, but for the eddy momentum flux convergence spectra in the shallow water model: (a) U_A = 10 m/s, (b) U_A = 20 m/s, and (c) the difference ((b)-(a)). The thick lines are the time and zonally averaged angular velocities at the upper layer (solid) and in the lower layer (dashed). The contour interval is 0.0075 m/s/day.